Chapter 16: Building Fire Hazard Predictions Using Machine Learning

Eugene Yujun Fu[1], Wai Cheong Tam[†,2], Tianhang Zhang[3], Xinyan Huang[3]

[1]Department of Rehabilitation Sciences, The Hong Kong Polytechnic University, Hung Hom, Hong Kong
[2]Fire Research Division, National Institute of Standards and Technology, Gaithersburg, Maryland, USA
[3]Department of Building Environment and Energy Engineering, The Hong Kong Polytechnic University, Hung Hom, Hong Kong

[†] Corresponding author: waicheong.tam@nist.gov

14.1 Introduction

In the period of 2015 to 2019, US fire departments responded to an estimated average of 346,800 home structure fires per year [1]. As compared to the estimate of 734,000 reported in 1980, the number of home structure fires is lower by approximately 50 % (i.e., an estimate of 356,500 in 2020). The reduction in home structure fires is possibly attributed by the presence of smoke alarms [2] and/or sprinkler systems [3-5], the use of fire-resistant building materials [6,7], better fire consumer education and awareness in fires [8,9], and the implementation of home safety codes [10-12]. However, the current home structure fires are more hazardous. In [13], experimental burns comparing spaces containing items common to modern homes and rooms with legacy furnishings were conducted. It is clearly seen that temperature rises rapidly for relatively shorter duration in case of fires in the modern (i.e., at ~ 5 min of fire in the modern room vs. after 29 min in case of the legacy room). This rapid temperature increase is largely due to the near-simultaneous ignition of most of the directly exposed combustible materials in the enclosed area. As seen in the figure, the temperature can exceed 800 °C in less than 20 seconds. This extreme fire event is known as flashover [14] and it presents an increased fire risks to the firefighters.

Backdraft is the abrupt burning of superheated gasses in a fire, caused when oxygen rapidly enters a hot, oxygen-depleted environment [15]. The backdraft explosion often happens when firefighters open a door or window of an enclosure room when conducting firefighting operation. The backdraft can occur without warning and is one of the most dangerous threats to firefighters' lives. According to statistics of 127 fire accidents involving explosions in different countries, 109 cases were related to the backdraft phenomenon [16]. Therefore, the dangerous

flashover and backdraft are major hazardous critical events in firefighting and raises the attention of fire researchers worldwide.

Currently, firefighters solely rely on their experience to detect critical fire events. There can be four warning signs [17] in a structure fire. Outside of the building structure, the presence of thick, black smoke and free-burning fires from windows and doors are two reliable signs of an impending flashover event. Inside the building structure, firefighters can try to seek for a fire phenomenon called rollover [17] near the ceiling and/or try to use their hands to feel the intense heat from the hot gas layer. However, these warning signs are generally difficult to be recognized accurately and it could take many years of experience to build up the necessary proficiency. Therefore, if the firefighters do not read flashovers correctly in time, their lives are in danger.

In the fire research community, a great deal of research efforts has been made to foster data-driven firefighting. Different methods are utilized to develop real-time fire hazard prediction models and these methods include empirical correlations [18-20], inversed modeling techniques [21,22], and computational fluid dynamics (CFD) based approaches [23,24]. Since the empirical correlations and the inversed modeling techniques use only closed-form mathematical expressions, these methods are easy to be implemented and are numerical efficient for quick evaluations. However, one drawback for these methods [18-22] is that they are limited to single-compartment structural settings and are not designed for multi-compartment structures. The CFD based approaches, such as [23], provide more flexibilities to account for structure variance and offer better prediction capabilities and higher prediction accuracy. Yet, the drawback of this kind of approach is that the models rely on high-performance computing machines and requires lengthy computations. As noted in [23], results from just one simulation time step takes more than five minutes to compute. Therefore, the CFD based approach at its current form will hardly be able to be used in real-time firefighting.

In addition, there is another drawback for the existing fire hazard prediction models. They do not account for realistic conditions from real fire scenarios. For example, the models [18-24] generally rely on both the continuous temperature signals from thermocouples in all compartments and the prior knowledge about the fire locations and vent opening conditions. However, fire protection devices, such as heat detectors, will stop functioning at elevated temperature [2] and the information about the fire locations and the opening conditions of windows and doors are often unknown. Since these realistic conditions (i.e., sensor temperature limit and the effect of arbitrarily fire location and vent opening conditions) have not been considered in the development process, the model performance from any of these models [18-24] is likely to be diminished. For that, a more robust data-driven approach is needed to overcome both the numerical challenge and the modeling complexity of realistic conditions from real fire scenarios.

Machine learning (ML) has made breakthroughs in various practical engineering problems, including human activity recognitions [25], recommendation systems [26], abnormal heartbeat classification [27], offline learning [28,29], intention detections [30], cooktop ignitions [31-33], and thermal radiation analyses [34-39].

ML paradigms have also been used extensively to overcome prediction challenges for various fire forecasting tasks. Chenebert et al. [40] provided a decision tree classifier for outdoor flame detections using image data. Yin and his co-workers [41] developed a deep neural network (DNN) framework for smoke detections. Another DNN model was developed and was used to identify flames for high-resolution videos given in residential building settings [42]. Aslan et al. [43] attempted to use generative adversarial networks for fire detections in large building structures using videos from surveillance cameras. The scientific advancement in ML truly enables reliable real-time predictions. However, these ML models might not be applicable to the current fire protection devices, such as heat detectors and smoke/CO detectors, where the data are in time-series. In order to fill in this knowledge gap, the Fire Research Division (FRD) from the National Institute of Standards and Technology (NIST) have collaborated with researchers from the Hong Kong Polytechnic University (HKPU) to develop ML technologies that can be used to enhance firefighters' situational awareness in built environments, protecting them from hazardous fire environments, and to pave the way for the development of data-driven prediction systems.

This chapter highlights the 4-year research efforts and the chapter is organized as follows. Section 2 describes the problem associate with the scarcity of real-life flashover data and the solution to overcome this data challenge. Section 3 presents the ML-based model development for flashover and backdraft predictions in residential settings. Finally, Section 4 summarizes the conclusions of the study and provides an overlook to future research directions.

14.2 Flashover Prediction by Numerical Database

To develop a robust ML-based prediction model, the dataset must contain sufficiently large amounts of relevant data that cover the desired ranges of fire conditions and geometric settings. Because flashover is an extreme fire event, the data collection is challenging. Unlike the classification tasks [44,45] and/or the regression tasks [46,47] being well established in the AI/ML community, the study of the flashover predictions for full-scale building structures in the ML domain has not been adequately addressed. For that, sensor data, such temperature, involving flashover in multi-compartment building structures is not available in any public data repositories such as [48]. Although fire data can be obtained by physically conducting the required full-scale experiments, when more complex building structures (i.e., with increasing number of compartments) and various realistic conditions (i.e., different fire and vent opening conditions) are needed to be accounted for, the required number of physical experiments is expected to be increased dramatically. When factors, such as cost and time, are of concern, physically conducting all full-scale experiments is not feasible. Therefore, in order to facilitate the development of ML-based flashover prediction models, the learning-by-synthesis approach is utilized for data collection.

The learning-by-synthesis (LBS) approach [49] provides an alternative means for data collection. To relate this concept to fire research, this approach makes use of computer simulation programs to conduct full-scale experiments with the desired fire and vent opening settings. Since the cost and time for running the numerical experiments are considerably lower than physically conducting the full-scale experiments, LBS provides flexibility to optimize the data quality through trial-and-error and to ensure the acquisition of a large amount of relevant data.

A series of research thrusts on the development of real-time flashover prediction models for residential building structures has begun since 2019 and these efforts have also been one of the primary research focuses for the smart fire fighting (SFF) project. The objective of this section is to describe the ML-based models that are developed to account for various realistic conditions encountered from real-life firefighting and how the fire problem is being addressed systematically.

There are three main challenges that the SFF project has overcome in terms of developing functional real-time flashover prediction models for residential building structures: 1) loss of data from sensors (i.e., heat detectors) at elevated temperature in a three-compartment home, 2) unknown fire conditions and venting opening configurations in a typical single-story residential home, and 3) application at-scale with different residential homes. Consequently, three different ML-based models are developed to address the three challenges: 1) P-Flash with SVR [50], 2) P-Flash with attention-based Bi-LSTM [51], and 3) FlashNet [52] and key information is presented in Sec. 16.3.1, Sec. 16.3.2, and Sec. 16.3.3, respectively. Readers are suggested to seek for complete details from the literature [50-52].

14.2.1 Zone-Model Fire Data Generation and Validation

A computational tool, CFAST Fire Data Generator (CData) [53,54], is developed to generate time series data for typical devices/sensors (i.e., heat detector, smoke detector, and other targets) in any user-specified building configurations. CData has three main modules: 1) preprocessor, 2) executor, and 3) accumulator.

Preprocessor Module: The preprocessor module is used to generate individual CFAST [55] input files. The CData input file utilizes the CFAST Namelist format. Seven different probability density functions are included to allow users to specify different simulation parameters, such as building layouts, surface materials, fire conditions, ventilation configurations, location of detector(s), and output intervals. Examples are provided in page 4 of reference [53]. Depending on the problem complexity and using approximately 200 nodes from a Linux cluster, approximately 10,000 CFAST cases can be completed in a day.

Executor Module: As part of the process of creating the individual CFAST inputs files, CData creates batch scripts for both Windows (see Pg. 25 from [54]) and Linux (see Pg. 26 from [54]) operating systems. Each batch script depends on external software to support running multiple CFAST jobs in parallel. Both of these scripts include information on the locations of these external files. With that,

running the set of CFAST simulations is accomplished by running the appropriate script for Windows or Linux. By default, a maximum of 100,000 iterations are set for each run to ensure that jobs which take an extremely long time to run do not prevent the rest from running. This value can be changed in both of the batch scripts.

Accumulator Module: A summary spreadsheet containing detailed information about all input parameters for each of the CFAST cases can be generated in this module. This spreadsheet can be used to carry out data inspection to eliminate any parameters. This information is crucial to ensure the quality and the covering range of the fire data. Readers who are interested in CData can refer to [54] for additional details and examples.

CData uses CFAST as the simulation engine. In general, CFAST is validated against more than 15 other sets of full-scale experiments [55] with peak heat release rate (HRR), compartment aspect ratio (i.e., compartment length against ceiling height), and global equivalence ratio, ranging from approximately 50 kW to 15,700 kW, 0.4 to 4.9, and roughly 0 to a value larger than 1 for a wide range of ventilation factors, respectively.

In order to ensure data fidelity in a more complex geometric setting, additional model validation is carried out. Specifically, temperature measurements obtained from two full-scale gas burner experiments (Exp 1 and Exp 2) reported in [56] are used to benchmark the synthetic temperature data generated using CFAST. Fig. 1a shows the floorplan of the single-story residential structure and it is consisted of a living room, kitchen, a dining room, a short hallway, and three bedrooms. The fire for both experiments is initiated at the living room and the heat release rate of the gas burner fires are the same for the two experiments.

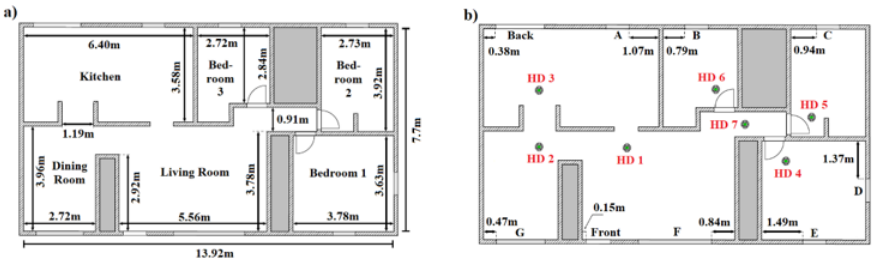

Fig. 1. Plan view dimensioned drawing of a) the single story structure and b) vent openings with heat sensors (HD) [56].

Fig. 2 show the upper gas layer temperature profiles for the two experiments. The blue solid lines represent the synthetic temperature data obtained from CFAST. The red dash lines are the estimated upper gas layer temperature for the experiments, and they are obtained based on the hot gas layer reduction method provided in [56]. It can be seen that the magnitudes and trends of the temperature profiles match the experimental data for different vent opening events. The window opening conditions can be retrieved from [51,57]. This observation indicates that

CFAST, the simulation engine of CData, is capable of capturing both the corresponding effect of fire and vent openings in the single story multi-compartment structure. In terms of uncertainty, the absolute root mean squared error is about 30 °C and 10 °C for Exp 1 and Exp 2, respectively. Comparison is also made for other compartments and the overall agreement is very good. Therefore, it can be expected that the generated temperature data can be reliably used for model development.

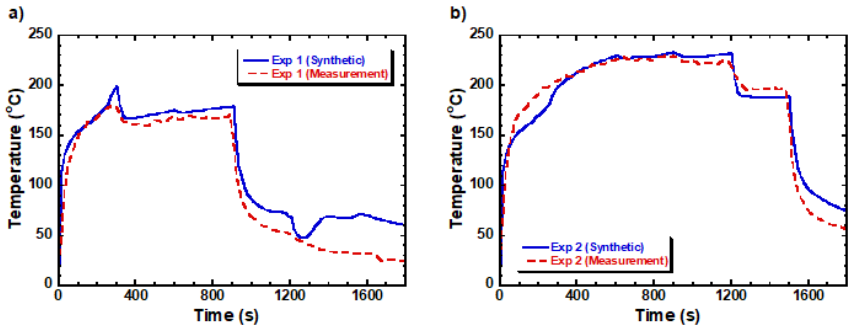

Fig. 2. CFAST validation against measurement for a) Experiment 1 and b) Experiment 2.

14.2.2 Flashover Prediction Using Recovered Temperature Data (P-Flash with SVR)

The primary question to be addressed in the first study is to develop a modeling framework that can be used to provide predictions even when temperature data are not available due to malfunctioning heat detectors at elevated temperature. The subsequent sections will provide discussion on: i) numerical setup for the three-compartment home, ii) corresponding temperature behaviors, iii) heat detector operational temperature limit, iv) flashover criteria, v) methods to overcome missing data, vi) model development of P-Flash, and vii) model performance.

Numerical Setup: Consider a single-story building with three compartments as shown in Fig. 3a, the dimensions of Room 1 are 3.5 m x 3.5 m, and the dimensions of Room 2 and Corridor are 4.5 m x 4.5 m and 3.5 m x 1 m, respectively. The ceiling height is 2.5 m, and it is identical for all compartments. For simplicity, the material of all walls, ceilings, and floors is gypsum wallboard. As seen in Fig. 3a, there are 4 openings: 1) a window in Room 1, 2) a door between Room 1 and Corridor, 3) a door between Corridor and Room 2, and 4) an exit-door in Room 2. The openings are fully opened. There is one heat detector in every compartment, and they are all located at the center of each compartment about 4.5 cm away from the ceiling. The response time index for the heat detector is 35 $(ms)^{0.5}$.

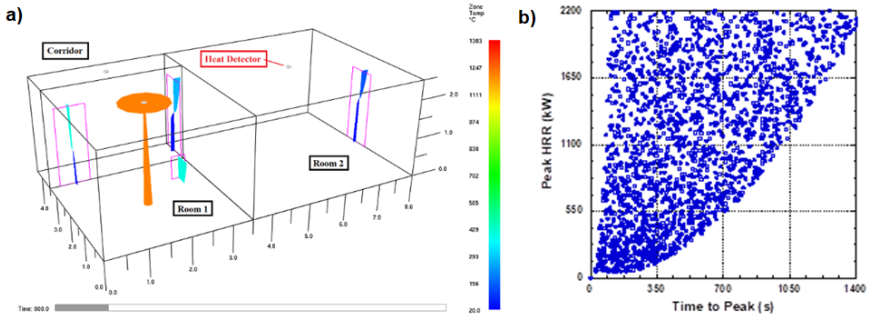

Fig 3. a) Schematic of the single-story three compartments with a fire in action and b) scatter plot for peak HRR vs time to peak.

Temperature Behaviors: CData is used to obtain 1000 different simulation runs with a t-squared fire at the center in Room 1. Based on references provided in [58], a range of fires are selected in this study. Fig. 3b shows the scatter plot of peak HRR and time to peak for the 1000 cases. It can be seen that the peak HRR and the time to peak ranges from approximately 50 kW to 2200 kW and from 50 s to 1400 s, respectively. The selected range of peak HRR and time to peak cover various burning items from an office trash can with a slow fire growth rate to an upholstered furniture fire with an ultra-fast fire growth rate.

For all simulation runs, a fire is started in Room 1. Subsequently, the upper layer gas temperature rises, and the layer thickness increases. Some hot gases leave the building structure, and some flow through the door. Air mixing between Room 1 and Corridor occurs. Due to the mixing, the upper gas layer temperature in Corridor also increases. Similar mass transfer and heat transfer processes take place between Corridor and Room 2, and the Room 2 upper gas layer temperature gradually rises. It can be imagined that the overall temperature profile from Room 1 for a given fire is likely to be the highest and the Room 2 overall temperature is going to be the lowest (see Pg. 4 from [50]).

Heat Detector Maximum Operational Temperature Limits: Loss of heat detector (HD) temperature signal is a realistic condition in actual fire scenarios and the HDs are very unlikely to survive at elevated temperature and would fail at temperatures well below the flashover conditions. According to NFPA 72 [2], heat sensing fire detectors are categorized into seven different classes with temperature classifications ranging from low to ultra-high, and the maximum operational temperature ranging from approximately 29 °C to 302 °C. In order to find a balance in between applicability and model challenge, the extra high class HD with a maximum operational temperature limit of ~ 150 °C is selected.

Flashover Criteria: Numerous variables can affect the transition of a compartment fire to full room involvement (i.e., flashover) [14]. Thermal influences including radiative and convective heat flux are assumed to be the driving forces and are clearly important. Ventilation conditions, compartment volume, and the chemistry

of the hot gas layer can also influence the occurrence of flashover. Based on the experimental studies reviewed in [14], the onset of flashover within a compartment can be quantified by two measurable criterions: 1) heat flux and 2) temperature. Peacock and his co-workers [14] demonstrated that when the incident heat flux onto the floor surface is between approximately 15 kW/m^2 to 33 kW/m^2, there can be a potential occurrence of flashover. However, the measurement of heat flux can rarely be measured in typical building environments because heat flux gauges are usually not installed. For that, the flashover criteria associated with heat flux cannot be used and it will not be considered in this study. For the temperature criterion, the range of values obtained from nine different literature sources in [14] ranges from 450 °C to 771 °C. The wide range of values for the temperature criterion is due to the large change in temperature within a very short period of time. Yet, it can be observed from [14] that most of the values are in the 550 °C to 650 °C range. To be conservative, the upper gas layer temperature of 600 °C is used as the threshold to determine the flashover moment.

Sequence Segmentation: Fig. 4 depicts the temperature profiles of a medium growth fire with high peak HRR case with a temperature cut-off at 150 °C. The dash lines are the ideal temperature profiles and the solid lines are the available temperature information. It can be seen that HDs begin to fail. There are only two and one remaining temperature information from the HDs in Phase II and Phase III, respectively. This missing temperature information imposes significant challenges for the model development and it is well known that developing a ML model based on unphysical data significantly jeopardizes the model performance. For that, the sequence segmentation is applied to the temperature data. There are three benefits from using the segmented data: a) the unphysical information due to any malfunctioning detectors is eliminated, b) the ML model can take full advantage of the available data associated with a specified phase, and c) the new data structure provides the basis for the model development of P-Flash.

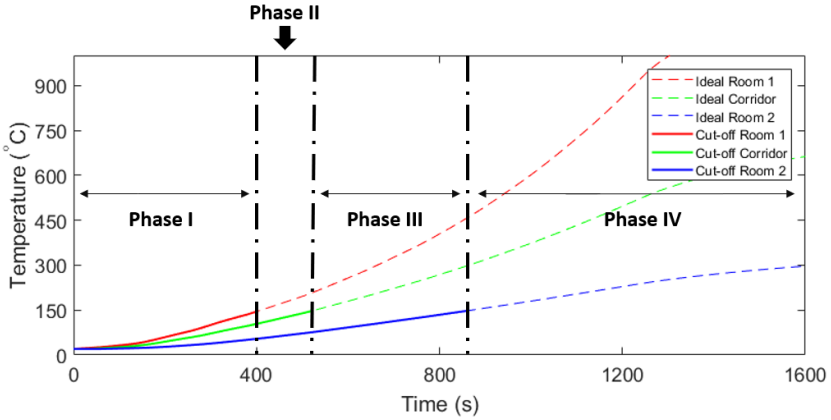

Fig. 4. Sequence segmentation and temperature profiles with 150 °C cut-off in 4 phases

P-Flash with SVR: A traditional machine learning algorithm, namely Support Vector Regression (SVR) [59], is used to develop the Prediction model for Flashover (P-Flash) to recover the missing temperature in different phases. Since SVR does not have capabilities to extract features itself, feature extraction is needed to obtain more useful features from the raw data. Two types of features are extracted for Phase I, II, and III and they are temperature-based features and trend-based features. These extracted features are the inputs and they help to build a more robust model. It should be noted that the list of extracted features can be found from page5 from [50].

Fig. 5 shows the overview of P-Flash model architecture. As seen in the figure, P-Flash is consisted of two regression models (R_{cor} and R_{R2}) and a memory component. ①, ②, and ③ are the extracted features. Both regression models, R_{Corr} and R_{R2}, are executed simultaneously and three outputs are obtained. Two temperature outputs from R_{Corr} and R_{R2} using features ① and ② are averaged to yield the recovered Room 1 temperature in Phase II and the recovered Room 1 temperature output for Phase III is directed obtained from R_{R2} using features ③. The Room 1 temperature information (Phase I to Phase III) is stored the memory component (M). Since temperature information is not available in Phase IV, curve fitting is carried out to extrapolate the missing temperature in Phase IV.

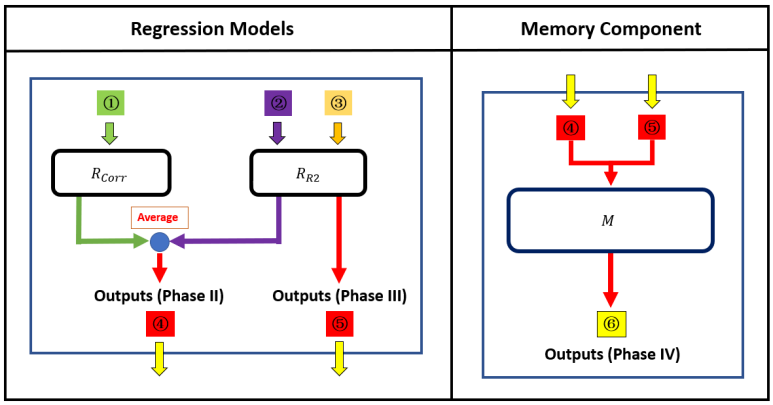

Fig. 5. Overview of model architecture for P-Flash.

Results and Discussion: Fig. 6 show the temperature predictions obtained from P-Flash for two selected cases: 1) a fast growth fire with low peak HRR case and 2) a medium growth fire with high peak HRR case. There are three sets of curves in each figure: i) ground truth/Room 1 temperature, ii) prediction with learning from fitting (LFF), and iii) prediction without LFF. For each prediction curve, it can be composed of up to two lines: a) red line represents the Room 1 temperature predictions associated with Phase II and III and b) blue line is for predictions in Phase IV. Since no prediction is needed for Phase I, comparison is omitted.

In Fig. 6a, it can be seen that P-Flash provides accurate temperature predictions of Room 1 in all phases, and the benefit of using LFF is noticeable. After approximately 1150 s, when all detectors are lost, P-Flash is still capable to provide predictions with similar trend and magnitude. For P-Flash without LFF, the prediction relies on the regression models, and it can be shown that the temperature prediction is unrealistic (i.e., showing a temperature increase to as high as 910 °C). This observation demonstrates that unphysical inputs will lead to unphysical outputs.

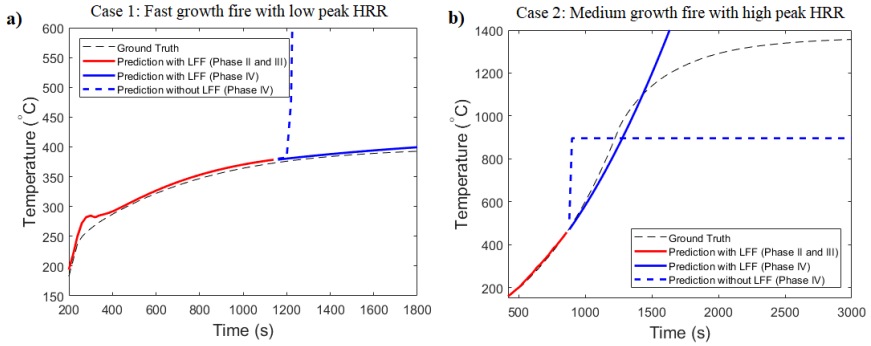

Fig. 6. Comparison between ground truth and predictions obtained from P-Flash a) with and b) without LFF.

In Fig. 6b, it can be seen that the temperature of Room 1 being recovered from Phase II and III is still growing exponentially. Since P-Flash does not have any information about the change of increase of the temperature, it over-predicts the Room 1 temperature significantly after ~ 1250 s. However, it should be noted that although P-Flash is capable to project the temperature increase in which the determination of flashover (i.e., temperature approaching 600℃) in Room 1 can be made, the model can only be applied for cases with fires at a fixed location and static (i.e., always open) vent conditions. In the following section, a more robust approach is presented. It is designed to account for arbitrary fire conditions and vent opening configurations in a realistic residential home and it is able to predict flashover for as many as 60 seconds before flashover occurs.

14.2.3 Flashover Prediction Using Surrogate Temperature Data (P-Flash with Attention-Based Bi-LSTM)

This section presents i) the numerical setup for the fire problem (an early flashover prediction task with a more complex building structure), ii) the unique temperature behaviors due to an arbitrary open door and the corresponding challenges, iii) the model development of P-Flash with attention-based Bi-LSTM, iv) results and discussion, and v) model limitations.

Numerical Setup: Consider a single-story ranch-style home structure as shown in Fig. 1a. There are seven major compartments: a living room, a dining room, a kitchen, three bedrooms, and a hallway connecting the living room and the three bedrooms. The overall interior dimensions of the structure are about 13.92 m x 7.7 m with a ceiling height of 2.44 m. The detailed dimensions associated with each of the compartments are shown in Fig. 1a.

Fig. 1b shows the relative position of the vent openings and the heat detectors in different compartments. For vent openings, there are two exterior doors (front and back), three bedrooms doors, and seven windows (from A to G). There is one heat detector (HD shown in Fig. 1b) located at each compartment and they are approximately 0.02 m away from the ceiling. The response time index of the HDs is similar to that mentioned in Sec. 16.2.2 and it is 35 $(m\text{-}s)^{0.5}$. The reason for selecting this single-story ranch-style structure is because about 90 % of residential buildings were built using this layout since the mid-1950s and this structure layout remains the most popular style of homes in 34 states across the United States [60]. For that, the research efforts with this structure are useful for the development process of real-time flashover predictions for firefighting across the U.S.

For each simulation case, there will only be one fire and it is either initiated at the center, against a wall surface, or at a corner within a compartment (except the hallway). The fire is located on the floor and this setting allows entrainment of oxygen-rich air and facilitates a more idealized condition for burning. A burning item is assumed to consist of four different fire growth stages and there is a linear growth (i.e., smoldering fire), t-squared growth (i.e., flaming fire), a peak, and a decay stage. Three items are considered and they are flaming chairs, polyurethane foam mattresses, and cotton-based mattresses. There items are found to be the leading items first ignited in home structure fires [1]. The transition HRR from smoldering to flaming fire (Q_1), peak HRR (Q_{max}), time to transition (t_1), time to peak HRR (t_2), peak time ($t_3 - t_3$), and decay time ($t_4 - t_2$) are summarized in Table 1. The peak HHR and time to peak HRR are obtained from [61], and the fire growth rate, α, is determined to be in between 0.000329 kW/s^2 and 0.041387 kW/s^2 which yields fires ranging from slow to fast fire growth rate.

For vent opening conditions, all doors and windows are initially closed and they can be opened based on the following two settings: a time-trigger setting for doors and a temperature-trigger setting for windows. For the time-trigger setting, the doors

Table 1. Approximate HRR parameters for chair and mattresses [61].

Items	Q_1 (kW)	Q_{max} (kW)	t_1 (s)	t_2 (s)	t_3-t_2 (s)	t_4-t_3 (s)
Chair	10 – 30	270 – 3500	150 – 1200	295 – 675	200	10
Mattress (foam)	10 – 30	2275 – 4620	150 – 1200	305 – 435	200	10
Mattress (cotton)	10 – 30	130 – 1670	150 – 1200	360 – 1240	200	10

in any compartments within the building structure can be opened at any given time within the t-squared fire growing stage. This setting allows mimicking door opening events due to activities, such as leaving the room of the fire origin and/or leaving the building structure. In addition, the arbitrarily open conditions of doors indirectly introduce double-peak fire growth behaviors that cannot be provided by just a simple t-squared fire.

The temperature-trigger setting allows windows to be arbitrarily opened when a temperature threshold is reached. In a fire scenario, a window is subjected to heating either from the local gas temperature and/or from the fire. Due to temperature or a flux gradient [62], a window may crack and eventually break out and create an opening to the outside environment. Based on [63], breakage of a single-pane float glass is experimentally observed at temperature between 100 °C and 200 °C. For that, when the window temperature reaches these thresholds (i.e., 100 °C – 200 °C), the window will then be opened. It is believed that the arbitrarily opening of doors and windows will provide more complex data behavior for development of a more robust ML-based model.

Temperature Behaviors and Challenges: Understanding the temperature data behaviors is vital to design a robust model architecture such that the ML-based prediction model is capable of learning the important relationship between temperature and flashover conditions. Fig. 7a shows temperature data for a double-peak fire case. Consider a fire occurs in Bedroom 1 with all the doors and windows in the building structure being initially closed. This setting creates a "sealed" compartment for Bedroom 1. As seen in the figure, the temperature first increases and then decreases due to the lack of oxygen. At around 470 s, the door is opened and the fire is approaching its peak. The temperature increases in bedroom 1, living room, kitchen, and dining room, but the temperatures in bedrooms 2 and 3 remain at ambient temperature. Physically, it is completely understandable because the doors are closed and the heated gases cannot enter the bedrooms. However, the modeling challenge presents here is that the information about the opening of the doors in not known in a real fire scenario. So, the model needs to learn to omit data that are not important. Fig. 7b shows the fire case with the heat detector maximum

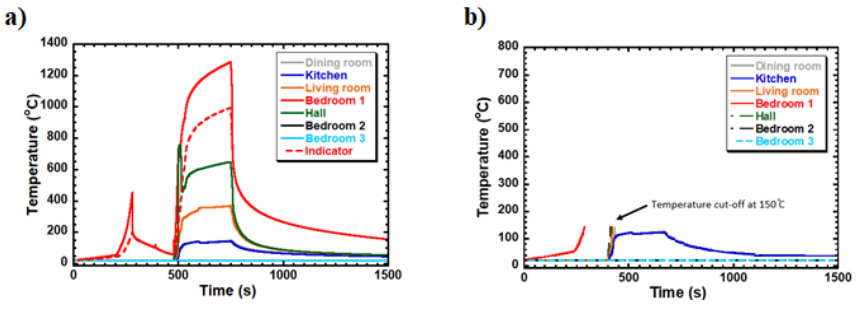

Fig. 7. a) Temperature profiles of different compartments for a ventilation-controlled fire case and b) temperature profiles with a cut-off value of 150 °C.

operational temperature limit at 150 °C. As shown in Fig. 7a, the flashover condition in the living room is met at about 500 s. Yet, the living room temperature is no longer available after ~ 300 s. Therefore, it can be seen that the model does not only need to discriminate data with higher importance, but it also needs to relate the temperature from other compartments for flashover conditions.

P-Flash with Attention-Based Bi-LSTM: In order to overcome the two abovementioned challenges, a bi-directional long short-term memory (Bi-LSTM) with self-attention mechanism is formulated. The Bi-LSTM algorithm [64] is to capture the complex data behaviors and the overall model structure is shown in Fig. 8a. The figure shows that for a temperature signal: $S = (s_1, s_2, \dots, s_\tau)$ and a time step i, Bi-LSTM includes a forward hidden state $\overrightarrow{h_i}$ and a backward hidden state $\overleftarrow{h_i}$. Since the complete behavior for temperature signals is needed, only the last hidden state of $\overrightarrow{h_\tau}$ and $\overleftarrow{h_\tau}$ are extracted from the Bi-LSTM. As shown in the figure, concatenation is applied to yield $h_\tau = [\overrightarrow{h_\tau}, \overleftarrow{h_\tau}]$ to encode temperature behavior with flashover conditions.

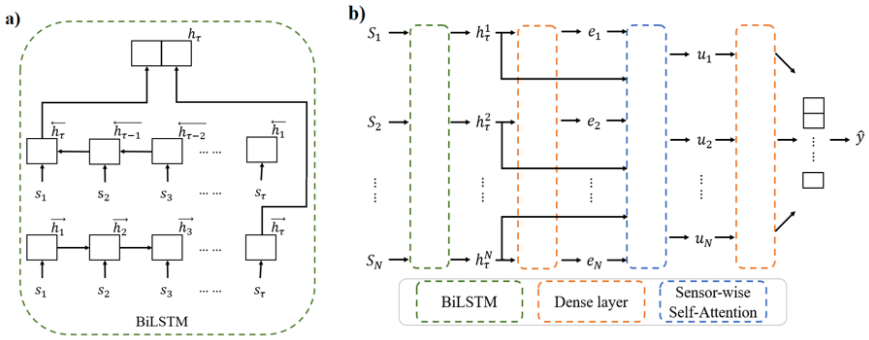

Fig. 8. a) Model architecture of BiLSTM and b) BiLSTM with sensor-wise self-attention.

In order to enhance the learning capability of the model in discriminating temperature signals with higher significance (i.e., neglecting bedrooms 2 and 3 temperature signal in Fig. 7b), a self-attention mechanism (see Fig. 8b) is used to model the sensor-wise relationships. With that, the contextual temperature information of all compartments within the structure can be extracted and it is believed that the contextual information can contribute to provide more accurate flashover predictions within the coming 30 s and 60 s based on the available temperature signals. Detailed mathematical formulations of the model are provided in page 6 from [51].

Results and Discussion: Table 2 shows the model performance for flashover predictions with a lead time of 30 s and 60 s. Based on the overall accuracy, the attention-based Bi-LSTM outperforms the original Bi-LSTM. The attention-based model also yields a significantly better recall score, indicating the benefits of

including the sensor-wise self-attention mechanism, and this is important because there are fewer false negatives for flashover events. As shown in Table 2, the overall performance for cases with a lead time of 60 s is generally better. One possible reason is due to the fact that it has a larger set of training samples.

Table 2. Performance of P-Flash.

x	Model	Acc.	Prec.	Rec.	F1
60s	BiLSTM	81.8%	86.9%	74.9%	80.5%
	BiLSTM-Attention	86.5%	84.6%	89.2%	86.8%
30s	BiLSTM	78.2%	77.0%	80.5%	78.7%
	BiLSTM-Attention	81.8%	79.5%	85.6%	82.3%

Fig. 9 illustrates the learned attention weights between the sensor signals in fire origin room and other compartments: kitchen (K), dining room (D), living room (L), and bedrooms 1 to 3 (B1, B2, B3), for two door opening conditions: all opened denoted as Open and all closed denoted as Close. As shown in the figure, the attention-based model can discover the spatial relation between sensor signals from different compartments. For example, when fire occurs in kitchen, the signal of dining room and living room are determined as the most discriminating surrogate signals (see Fig. 9a). This is expected because the sensors placed in these two rooms are very close to the kitchen. On the other hand, the signals from dining room and kitchen are barely important for our model when fire occurs in bedroom 1, regardless of the door opening conditions (see Fig. 9b). This also agrees with their spatial relations that the sensors in dining room and kitchen are farer away from that in bedroom 1. It can be seen that the learned attention weights suggest that the attention-based model can effectively learn the useful relationships between different sensor signals under different door opening conditions without the need of providing any prior information.

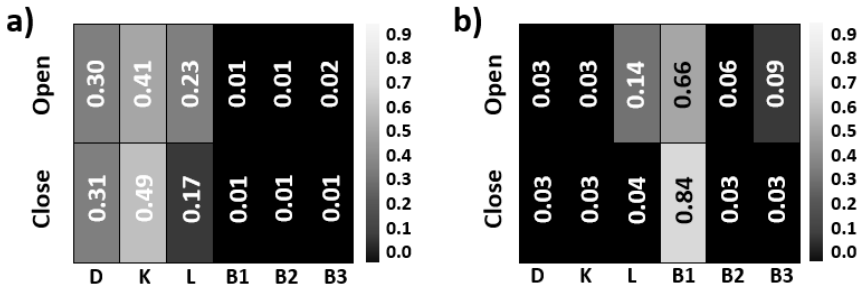

Fig. 9. Learned attention for a) Kitchen and b) Bedroom 1, under different door opening conditions.

Limitations: One major limitation of existing prediction models such as [50, 51] lies in their generalizability across different building structures. The model architecture from these models does not support a variable number of input data and floorplans. For example, a model trained for one building structure with 3 channels of temperature data (Fig. 4) does not generalize to another with 7 channels (Fig. 7). This model limitation imposes the need of prior knowledge about the exact floorplan of the building structure. However, this kind of information is usually unknown in practical firefighting.

14.2.4 Generic Flashover Prediction Model (FlashNet)

This section presents the model development efforts to account for a wide range of residential homes with different floorplans and this section includes 4 subsections: i) the home structures, ii) the concept of graph structured data, iii) the model formulation for FlashNet, and iv) results and discussion.

Home Structures and Numerical Settings: Seventeen typical single-floor home structures are selected from [65], which defines 209 dwellings to represent approximately 80 % of U.S. housing layouts. These 17 structures can be categorized into three types of residential buildings: 1) apartment homes, 2) attached homes, and 3) detached homes . The overall floor area ranges from 65 m^2 to 275 m^2 with three to fourteen compartments.

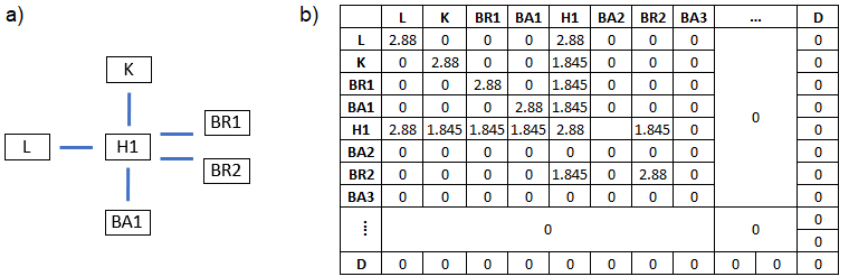

	L	K	BR1	BA1	H1	BA2	BR2	BA3	...		D
L	2.88	0	0	0	2.88	0	0	0			0
K	0	2.88	0	0	1.845	0	0	0			0
BR1	0	0	2.88	0	1.845	0	0	0			0
BA1	0	0	0	2.88	1.845	0	0	0	0		0
H1	2.88	1.845	1.845	1.845	2.88		1.845	0			0
BA2	0	0	0	0	0	0	0	0			0
BR2	0	0	0	0	1.845	0	2.88	0			0
BA3	0	0	0	0	0	0	0	0			0
⋮	0								0		0
											0
D	0	0	0	0	0	0	0	0	0	0	0

Fig. 10. A schematic of a) a graph representation and b) an adjacency matrix for the six-compartment home.

Graph Structured Data: The graph structured data is made up of two components: node attribute matrix which is the extracted instances for temperature and adjacency matrix. The adjacency matrix is formulated using two steps. The first step is to convert the home floorplan into a graph representation. An example is shown in Fig. 10 where each compartment is represented by a node and the corresponding opening or connection between two compartments is represented by an edge. The non-diagonal matrix elements are determined based on the size of opening between two compartments (i.e., the height and the width of a door from a bedroom to the

hallway). For the diagonal elements, since the temperature information is crucial to correlate the potential occurrence of flashover, they are taken to be the maximum value of the non-diagonal elements. For the six-compartment building structure, the maximum value is 2.88 m^2. The same procedure is carried out to generate the graph representations for the rest of the sixteen building structures.

The second step is to obtain a geometric averaged adjacency matrix (GAAM) that can be used for all home structures. By visual inspection of the seventeen building structures from [52], there can be a possible of 15 x 15 compartment combinations a living room (L), kitchen (K), bedroom1 (BR1), bathroom1 (BA1), hall1 (H1), bathroom2 (BA2), bedroom2 (BR2), bathroom3 (BA3), den (Den), bedroom3 (BR3), family room (Fam), bedroom4 (BR4), hall2 (H2), hall3 (H3), or a dining room (D). The use of this information provides the dimensions of the GAAM. Final GAAM matrix elements are determined using the statistical mean of the normalized adjacency matrices from the seventeen home structures. Additional explanation for the determination of GAAM and the corresponding GAAM for the fourteen-compartment detached home are provided in page 6 to 7 in [52].

Model Formulation: The overall structure of the Flashover prediction neural Network , namely *FlashNet*, is presented in Fig. 11 and the model has a single block of a spatial temporal graph convolutional network (ST-GConvN). The ST-GConvN block is used to capture the spatial and the temporal dependencies from the multivariate temperature data and consists of two temporal convolution layers and one spatial graph convolution layer. The required number of layers is determined based on numerical experiment [47]. For each temporal convolution layer, there is a 1-D convolution following by a rectified linear unit (ReLU), and this operation provides additional non-linearity to the temporal convolution layer to learn important features/information (i.e., how fast the temperature increase, how much time it takes to reach a certain temperature condition, etc.) in the time domain.

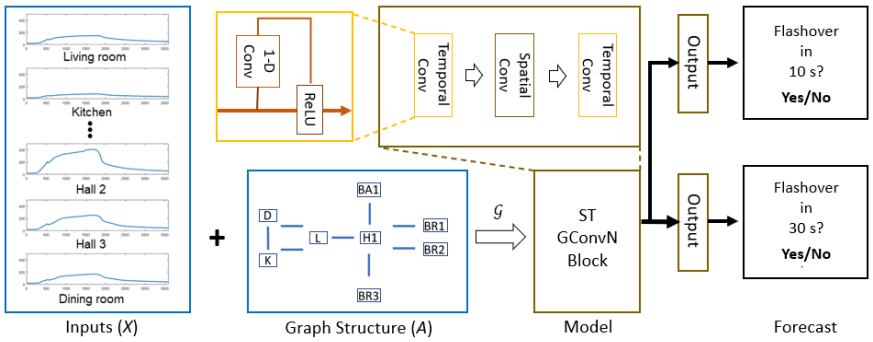

Fig. 11. Model structure of FlashNet.

Model Performance and Benchmarks: Table 3 shows the results for flashover prediction with a lead time of 10 s. FlashNet is benchmarked against five state-of-the-art prediction models. The baseline models include i) P-Flash with SVR [50], ii) MLP – a feedforward multiple-layer perceptron [66], iii) LSTM – a two-layer long short-term memory [67], iv) P-Flash with attention-based Bi-LSTM [51], and v) CNN – a three-layer standard convolutional neural network [68]. As shown in Table 5, FlashNet outperforms the existing machine learning based prediction models and achieves an overall accuracy of about 85.2 %. Also, the scores from precision, recall, and F1 suggest that FlashNet is a well-balanced model which minimizes the false positive and the false negative. The main reason why FlashNet improves the model performance is that the nature for temperature data in flashover predictions accounting for different building structures with a wide range of fire and vent opening conditions is better suited for the modeling assumptions about temporal and spatial dependencies. In terms of training time, most of models, except ANN and the linear SVM, require about 30 minutes for convergence. For testing, models generally take about 3 seconds to make predictions for testing subset. On average, one prediction uses about a fraction of a second per instance.

Table 3. Baseline comparison against five existing machine learning based flashover prediction models.

Methods	Acc.	Prec.	Recall	F1	Training (s)	Testing (s)
SVM	53.6%	52.8%	66.6%	58.9%	37.5	0.01
MPL	62.1%	49.4%	74.3%	59.3%	710.6	2.42
LSTM	66.6%	75.7%	49.7%	60.1%	1594.1	2.87
BiLSTM-ATT	70.0%	66.6%	81.2%	73.2%	1834.8	2.93
CNN	79.8%	85.0%	74.8%	79.5%	1351.0	2.38
FlashNet	85.2%	83.5%	87.8%	85.6%	1657.3	2.91

14.3 Flashover and Backdraft Prediction Using Real Data

Section 16.2.1 to Sec. 16.2.4 presents the machine learning model development using synthetic fire data. In this section, the development of the deep learning model uses real fire data from both small and real scale chamber fire experiments. Similar to the previous sections, descriptions for the experimental setup and the data behavior are first given. Then, the model formulations and important observation are presented.

14.3.1 Flashover forecast in Scaled Room Fire Tests

This study [67] considers a standard 1/5th scale cubical enclosure with side lengths of approximately 0.5 m. The enclosure is primarily constructed with 4 mm thick galvanized steel. In order to observe the fire growth, a refractory glass is installed on the right side of the enclosure. In additional, there is an adjustable opening in the front side of the enclosure. Within the enclosure, three thermocouples are placed, along the centerline, on the ceiling. The first thermocouple is about 0.05 m away from the front opening and the second and third thermocouples are about 0.2 m apart. Two digital cameras are placed outside of the enclosure to visualize the fire development and to determine when there is an onset of flashover.

A series of experiments is carried out. There are 11 pool fire experiments and 13 wood crib fire experiments. Six different vent opening conditions are considered. Fig. 15 shows the temperature growth from the three thermocouples for a) a 24 cm diameter liquid pool fire with 0.4 m (height) x 0.16 m (width) opening and b) a large wood crib fire with 0.2 m x 0.3 m opening. It can be seen in these figures that temperature data from real fire test has noticeable temperature oscillations. This kind of temperature behavior is missing from the synthetic temperature data generated by a zone model (i.e., CFAST). In Fig. 12, there are four primary fire stages: 1) growing, 2) flashover, 3) fully developed, and 4) decay. Video recordings are used to determine the onset of flashover. Specifically, when spilled flame is noted, the corresponding timestamp is marked as flashover. For example, the onset of flashover in Fig. 12a is about 320 s.

Model Formulation: The deep learning (DL) model carries out the following two tasks: 1) temperature prediction as a regression task and 2) flashover prediction as a binary classification task. Fig. 13 depicts the overall workflow and the model structure of the DL model. The model inputs are the temperature profiles from the three thermocouples. A rolling time window of 20 s is used to facilitate real-time, continuous forecasts and the z-score normalization is conducted to normalize the

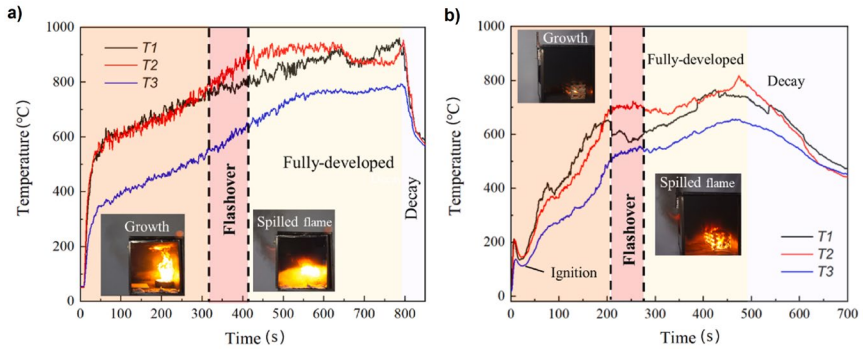

Fig. 12. Typical temperature growth for different fuels (a) 24-cm diameter liquid pool fire with 0.4 m × 0.16 m opening and (b) large wood crib fire with 0.2 m × 0.3 m opening.

input data in the same scale. Input data is divided into three subsets and they are training, validation, and testing subsets.

As seen in Fig. 13, the DL model is consisted of a stacked Long Short-Term Memory (LSTM). The 1st LSTM has a state number of 120 and the 2nd LSTM has a state number of 80. A dropout of 0.2 is applied to both LSTM layers to facilitate training stability. The extracted features obtained from the LSTM layers are passed to a fully connected layer with a node number of 64. Relu is used to provide additional nonlinearity for mapping. Depending on the forecasting task, the output layer for the temperature prediction and the flashover prediction has a node number of 3 and 1, respectively.

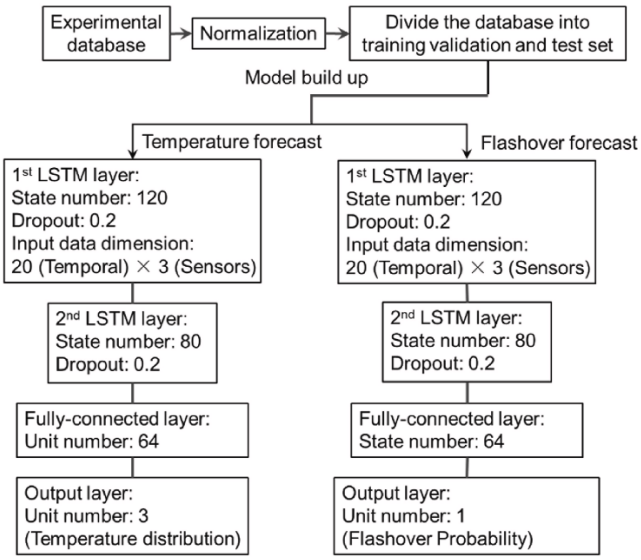

Fig. 13. The structure of the LSTM based fire forecast model.

Results and Discussion: Figure 14 shows the predicted results of the DL model for a large wood crib fire with 0.2 m × 0.3 m opening. Specifically, the temperature forecast and the forecasting flashover probability with a lead time of 10 s are shown in Fig. 14a and Fig. 14b, respectively. The solid lines are the ground trues and the dash lines are the model predictions. For temperature forecast, it can be seen from Fig. 17a that the DL model is capable to predict the future temperature (with a lead time of 10 s) and the temperature predictions capture the trend of the temperature growth. For this particular case, the overall discrepancy between the predictions and the ground true is about 10 %. In term of flashover prediction, it can be seen that the model has relatively promising performance and it can forecast the potential occurrence of flashover correctly. The results from this study affirm a fact that machine learning paradigm can learn the important patterns for various prediction

tasks such as temperature and flashover predictions from real fire temperature data that has various noise and temperature fluctuations.

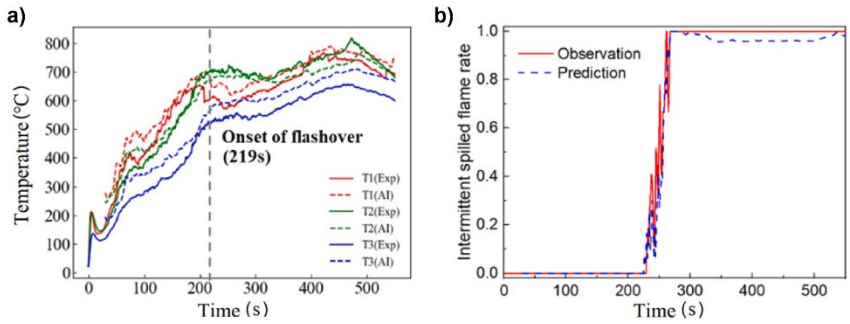

Fig. 14. Model prediction of a) temperature and b) flashover probability for a large wood crib fire with 0.2 m × 0.3 m opening.

It is hoped that these research efforts can continuously overcome limits and/or eliminate assumptions that the traditional modeling approaches fail to capture. In the next section, another thrust of research efforts is presented to highlight the current modeling advancement in other built environments.

14.3.2 Predicting Backdraft in Real-scale Room

This section presents a full-scale fire test in a 5.5 m (length) x 2.4 m (width) x 2.4 m (height) chamber (Fig. 15). Wood planks are adopted as the fuel and arranged to simulate the furniture, room ceiling, sidewalls, and floor to simulate the fuel distribution in an actual building environment (Fig. 15a-b). At the beginning of each test, an advanced flame-thrower burner is employed to ignite the innermost fuel until the fire can sustain itself autonomously. When the fire grows to large enough, the door is then closed to create a nearly sealed room environment. After the fire further developed inside the room for a certain period, the door can be opened to generate a spilled flame or a backdraft. The operation of close and open door is repeated several times in each fire test with different internal fire scenarios (varied oxygen supply and fire HRRs) and door enclosure durations to obtain backdraft samples with various intensities.

Totally, five groups of large-scale fire tests are conducted on different dates under varied ambient and weather conditions. Each test includes multiple spilled flame and backdraft processes. The temperature profile in each experiment is measured by a set of thermocouple arrays (Fig. 15c). Two TC trees (TC#1–6 and TC#13–18) are adopted to record the vertical temperature distribution, and these data can be used to identify the smoke stratification. The horizontal TC array (TC#7–12) are set to measure the temperature distribution of the upper smoke layer. Moreover, two fixed cameras and a camera carried by portable Unmanned Aerial

Vehicle (UAV) are installed a few meters away from the chamber door to record the smoke and flame videos from different view angles.

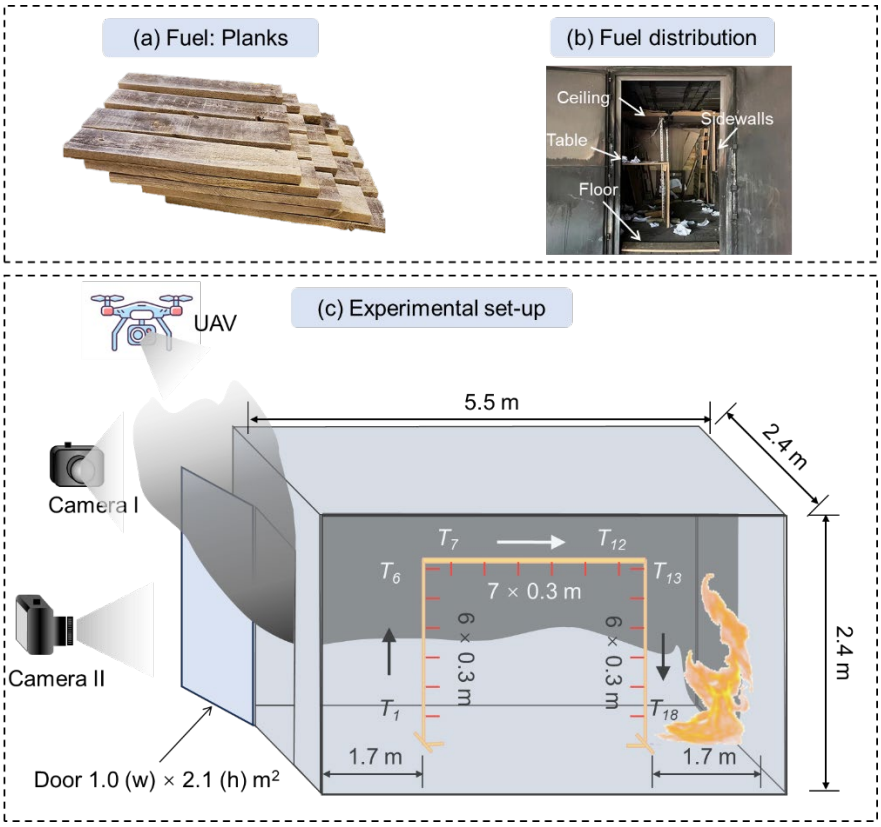

Fig. 15. Experimental setup of the full-scale backdraft test chamber.

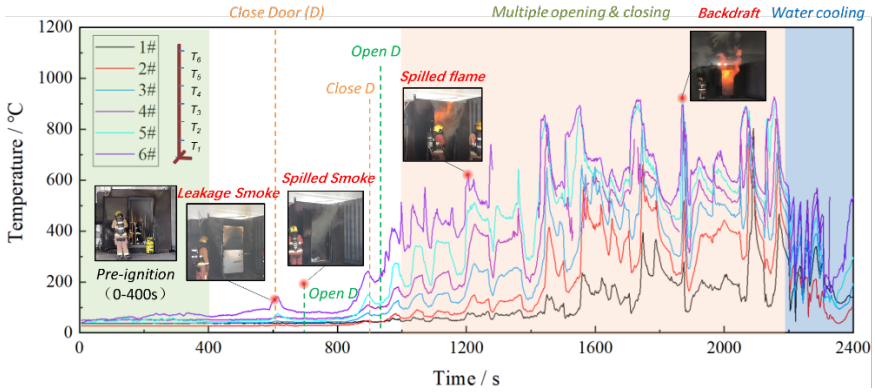

Fig. 16. Experimental setup of the full-scale backdraft test chamber.

The typical temperature growth of the large-scale fire test is plotted in Fig. 16. As shown, when closing (opening) the door, the oxygen will be cut off (supplied) to induce the temperature decay (rise), respectively. When the fuel gas concentration and the internal temperature reach a critical level, an explosion will happen when the door is open. This explosion is a typical backdraft phenomenon. During the period of 1000 – 2200 s, the door is closed and re-opened several times. Then, several no-backdraft cases and backdraft cases with different intensities are further observed, depending on different initial states (e.g., the previous door-close duration and internal temperature) and door enclosure durations. Finally, the fire is either extinguished with a fire hose or continued until the burnout of fuel (the blue region). In total, 31 times of backdrafts have been observed in 5 tests.

Model Formulation: Unlike other critical event in the building fire, which is the spontaneous evolution of the fire system, the occurrence of the backdraft is associated with the firefighter's action, i.e., open or close the door so the state of the chamber is important information to judge the backdraft risks. Therefore, a multimodal deep learning framework to integrate the sensor signal (temperature) and visual signal (images) are proposed to forecast the backdraft (Fig. 17). The original transformer and Vision-transformer algorithms are adopted as the encoder for the sensor data and visual data, respectively. The input image is first divided into a grid of patches and linearly embedded into a lower-dimensional vector representation. The patch embeddings are then passed through a series of transformer encoder layers (four in this work for the visual signal). In each layer, two key components, i.e., self-attention and feed-forward neural networks, are adopted to capture both local and global dependencies among the patches. Similarly, the sensor data are also processed by transformer encoder layers (two in this work) to extract the features and dependencies.

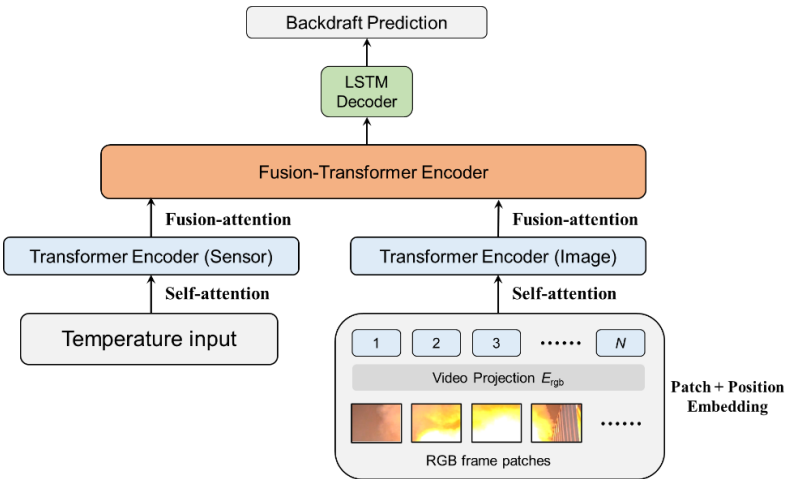

Fig. 17. Diagram of the Fusion-transformer structure.

After the initial encoding of each modality, a cross-modal attention mechanism is employed in the fusion-transformer layer, in which the attention scores between the representations of different modalities, allowing them to attend and exchange information with each other. In this study, the model tries to link the temperature variation characteristics (absolute value and gradient) with the firefighter's operation (closing or opening the door) and establish potential connections among these features. Finally, the fusion-encoded information from multimodal data passes through the LSTM model to obtain the temporal features, and two fully connected layers are used to achieve the nonlinear fitting and generate the output, namely, the backdraft intensity (represented by the maximum explosion flame height).

Results and Discussion: Figure 18 presents the prediction of the deep learning model for backdraft onset with ground truth. As shown, there are eight times of close-open cycles in the whole experiment, and seven of them successfully induce a backdraft with different intensity while the last time has no backdraft due to the water-cooling effect. Accordingly, the proposed model predicts a certain backdraft intensity for the seven samples which successfully generate a backdraft and outputs a zero for the last time with the water cooling. The model performs a 100 % accuracy on predicting the occurrence of the backdraft with a low delay time (less than 1.6 s). Meanwhile, the accumulation of the pyrolysis fuel gas and the gradual temperature decay can well be reflected by the increase and decrease of predicted backdraft risk, respectively, indicating that the results are phenomenological.

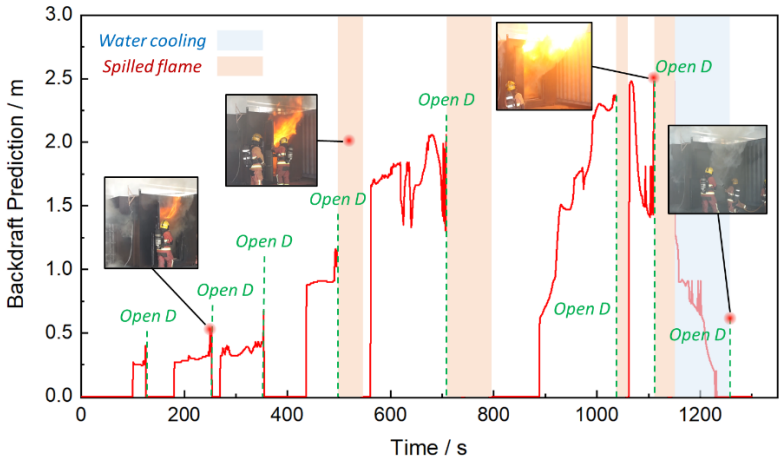

Fig. 18. Deep learning model prediction VS observed ground truth.

14.4 Challenges and Perspectives in AI-Driven Fire Forecast

14.4.1 Challenges

Interpretability of the AI/ML fire modeling. Despite the numerical advantages from [50-52], there is one sufficient drawback of using ML paradigm and that is, the models are not interpretable. Often time, it is considered as a black box. It is well understood that being able to explain the model decision is important for practical engineering applications, especially when the potential applications involve lives. Also, model interpretability provides traceable information to scientists or engineers to understand the underlying reasons why a model is making such a correct or a wrong decision. In the future study, an explainable ML-based flashover prediction model is needed and model interpretability can be introduced using various techniques such as feature attention mechanism, feature visualization, and/or class activation map [69]. These techniques can help to extract discriminative information in both spatial and temporal domains for the multivariate series so that a more trust-worthy ML system can be developed to address the fire safety problems.

Lack of consistent criteria of critical events. As demonstrated above, many phenomena (critical temperature, heat flux, spilled flame, rollover, etc.) can be regarded as the flashover onset but a large difference in the predicted moment may be caused by the adaptation of those criteria. For example, according to the temperature profile in a 1/5 scaled model fire test, the average ceiling temperature can reach 600 ℃ in around 120 s, whereas if the visual criterion, spilled flame is utilized, the flashover occurs at around 220 s, which is around 100 s later than the temperature data-based prediction. Therefore, although many papers claimed that they are predicting the flashover onset, they are indeed forecasting different moments if there is not a consistent definition. Consequently, the prediction results with different models are not comparable, which largely impedes the communication and spread of smart forecast models.

Lack of a comprehensive database. Compared with engineering applications in other fields, data collection for fire research is always a big challenge. Full-scale fire test data are of great significance as they are closest to real fire accidents but very dangerous and costly at the same time. In contrast, the scaled model and numerical tests are friendly for both money and time, which is a better way to generate a large amount of data for AI training. However, the results from scaled and numerical models are inevitably affected by the scaling effect and simplifying assumptions. Since the prediction accuracy of the AI model relies heavily on the quality of the database, the performance of the AI model trained by the ideal database is always questionable.

14.4.2 Perspectives

Vision-based fire scenario recognition. Compared with sensor data, which is hard to access in real fire incidents, the visual data are more accessible as they can be captured by potable cameras, Unmanned Aerial Vehicles (UAVs), and even the cell phone of residents. Computer vision technology shows a good performance to identify the fire Heat Release Rate (HRR) based on the external smoke [70] and flame images [71,72]. Combined with remote sensing technologies, the vision-based deep learning model is expected to provide more useful fire scene information, such as the fuel load, fuel type, potential fire spread path, and thus help predict the fire evolution and critical events occurrence accurately.

Physics-guided model training. The issue of interpretability and lacking large-scale fire test data is expected to be solved by physics-guided model training, which is proposed to address the data imbalance problem. The principle is to introduce physical knowledge, e.g., the scaling law, government equations, and fire dynamics in the training process. To be more specific, the closed-form and partial differential physical equations are served as a term in the loss function with a certain weight or embedded in each layer to impact the training process directly. Then the multi-source fire test data can be well understood by AI.

References

1. Ahrens, M., & Maheshwari, R. (2021). Home Structure Fires. National Fire Protection Association. Quincy, MA 02169.
2. NFPA 72. National Fire Alarm and Signaling Code. (2022). National Fire Protection Association. Quincy, MA 02169.
3. NFPA 13. Standard for the Installation of Sprinkler Systems (2022). National Fire Protection Association, Quincy, MA 02169.
4. NFPA 13D. Standard for the Installation of Sprinkler Systems in One- and Two-Family Dwellings and Manufactured Homes. (2022). National Fire Protection Association, Quincy, MA 02169.
5. NFPA 13R. Standard for the Installation of Sprinkler Systems. (2022). National Fire Protection Association, Quincy, MA 02169.
6. Wilkie, C. A., & Morgan, A. B. (Eds.). (2009). *Fire retardancy of polymeric materials*. CRC press.
7. Kodur, V., Kumar, P., & Rafi, M. M. (2019). Fire hazard in buildings: review, assessment and strategies for improving fire safety. *PSU Research Review*.
8. Chandler, K. M., Crown, E. M., & Brown, S. A. (1991). Consumer information and education effects on knowledge and choice of fire resistant upholstery. *Journal of consumer affairs*, *25*(2), 339-357.
9. FEMA. Fire-Safe Seniors Program. https://www.usfa.fema.gov/prevention/outreach/fire_safe_seniors.html, last accessed: 2022/12/13.
10. NFPA 220. Standard on Types of Building Construction (2021). National Fire Protection Association, Quincy, MA 02169.
11. NFPA 720. Standard for the Installation of Carbon Monoxide(CO) Detection and Warning Equipment. (2015). National Fire Protection Association, Quincy, MA 02169.

12. NFPA 70. National Electrical Code. (2023). National Fire Protection Association, Quincy, MA 02169.
13. Kerber, S. (2012). Analysis of changing residential fire dynamics and its implications on firefighter operational timeframes. Fire technology, 48(4), 865-891.
14. Peacock, R. D., Reneke, P. A., Bukowski, R. W., & Babrauskas, V. (1999). Defining flashover for fire hazard calculations. *Fire Safety Journal*, *32*(4), 331-345.
15. Drysdale, D. (2011). *An introduction to fire dynamics*. John wiley & sons.
16. Croft, W. M. (1980). Fires involving explosions—A literature review. *Fire Safety Journal*, *3*(1), 3-24.
17. Kim, H. J., & Lilley, D. (1999, January). Comparison of theories for room flashover. In *37th Aerospace Sciences Meeting and Exhibit* (p. 343).
18. Babrauskas, V. (1980). Estimating room flashover potential. Fire Technology, 16(2), pp.94-103.
19. McCaffrey, B.J., Quintiere, J.G. and Harkleroad, M.F. (1981). Estimating room temperatures and the likelihood of flashover using fire test data correlations. Fire Technology, 17(2), pp.98-119.
20. Kim, H.J. and Lilley, D.G. (2002). Flashover: A study of parameter effects on time to reach flashover conditions. Journal of propulsion and power, 18(3), pp.669-673.
21. Overholt, K. J., & Ezekoye, O. A. (2012). Characterizing heat release rates using an inverse fire modeling technique. Fire Technology, 48(4), 893-909.
22. Price, M.D. (2014). Using inverse fire modeling with multiple input signals to obtain heat release rates in compartment fire scenarios (Doctoral dissertation, University of Maryland, College Park).
23. Jahn, W. (2017). Using suppression and detection devices to steer CFD fire forecast simulations. Fire Safety Journal, 91, pp.284-290.
24. Koo, S.H., Fraser-Mitchell, J. and Welch, S. (2010). Sensor-steered fire simulation. Fire Safety Journal, 45(3), pp.193-205.
25. Fu, Y., Leong, H. V., Ngai, G., Huang, M. X., & Chan, S. C. (2017). Physiological mouse: Toward an emotion-aware mouse. *Universal Access in the Information Society*, *16*(2), 365-379.
26. Wang, Y., Chan, S. C. F., Leong, H. V., Ngai, G., & Au, N. (2016). Multi-dimension reviewer credibility quantification across diverse travel communities. *Knowledge and information systems*, *49*(3), 1071-1096.
27. Li, J., Brown, C., Dzikowicz, D. J., Carey, M. G., Tam, W. C., & Huang, M. X. (2023). Towards real-time heart health monitoring in firefighting using convolutional neural networks. *Fire Safety Journal*, *140*, 103852.
28. Levine, S., Kumar, A., Tucker, G., & Fu, J. (2020). Offline reinforcement learning: Tutorial, review, and perspectives on open problems. *arXiv preprint arXiv:2005.01643*.
29. Li, C., Wang, Y., Li, D., Chu, D., & Ma, M. (2021). An effective method of evaluating pension service quality using multi-dimension attention convolutional neural networks. *International Journal of Software Engineering and Knowledge Engineering*, *31*(04), 533-543.
30. Kwok, T. C., Fu, E. Y., Wu, E. Y., Huang, M. X., Ngai, G., & Leong, H. V. (2018, March). Every little movement has a meaning of its own: Using past mouse movements to predict the next interaction. In *23rd International Conference on Intelligent User Interfaces* (pp. 397-401).
31. Ngai, M., Fu, E., Tam, A., Yang, A., & Ngai, G. (2022). Finding the Signal from the Smoke: A Real-Time, Unattended Fire Prevention System Using 3D CNNs. *Journal of Student Research*, *11*(3).
32. Mensch, A. E., Hamins, A., Tam, W. C., Lu, Z. J., Markell, K., You, C., & Kupferschmid, M. (2021). Sensors and machine learning models to prevent cooktop ignition and ignore normal cooking. *Fire technology*, 1-24.

33. Tam, W. C., Fu, E. Y., Mensch, A., Hamins, A., You, C., Ngai, G., & Leong, H. (2021). Prevention of cooktop ignition using detection and multi-step machine learning algorithms. *Fire safety journal*, *120*, 103043.
34. Yuen, W. W., Tam, W. C., & Chow, W. K. (2014). Assessment of radiative heat transfer characteristics of a combustion mixture in a three-dimensional enclosure using RAD-NETT (with application to a fire resistance test furnace). *International Journal of Heat and Mass Transfer*, *68*, 383-390.
35. Tam, W. C., Yuen, W. W., & Chow, W. K. (2016). Numerical study on the importance of radiative heat transfer in building energy simulation. *Numerical Heat Transfer, Part A: Applications*, *69*(7), 694-709.
36. Yuen, W. W., Chow, C. L., & Tam, W. C. (2016). Analysis of radiative heat transfer in inhomogeneous nonisothermal media using neural networks. *Journal of Thermophysics and Heat Transfer*, *30*(4), 897-911.
37. Tam, W. C., Tam, W. C., & Yuen, W. W. (2019). *OpenSC: An Open-source Calculation Tool for Combustion Mixture Emissivity/absorptivity*. Gaithersburg, MD, USA: US Department of Commerce, National Institute of Standards and Technology.
38. Yuen, W. W., & Tam, W. C. (2020). Point mean beam length, a new concept to enhance the computational efficiency of multidimensional, non-gray radiative heat transfer. *Numerical Heat Transfer, Part B: Fundamentals*, *79*(3), 113-129.
39. Yuen, W., & Tam, W. C. (2022). A fundamental assessment of the concept of mean beam length for application for multi-dimensional non-gray radiative heat transfer. *International Journal of Thermal Sciences*, *179*, 107681.
40. Chenebert, A., Breckon, T. P., & Gaszczak, A. (2011, September). A non-temporal texture driven approach to real-time fire detection. In *2011 18th IEEE international conference on image processing* (pp. 1741-1744). IEEE.
41. Yin, Z., Wan, B., Yuan, F., Xia, X., & Shi, J. (2017). A deep normalization and convolutional neural network for image smoke detection. *Ieee Access*, *5*, 18429-18438.
42. Shen, D., Chen, X., Nguyen, M., & Yan, W. Q. (2018, April). Flame detection using deep learning. In *2018 4th International conference on control, automation and robotics (ICCAR)* (pp. 416-420). IEEE.
43. Aslan, S., Güdükbay, U., Töreyin, B. U., & Cetin, A. E. (2019). Deep convolutional generative adversarial networks based flame detection in video. *arXiv preprint arXiv:1902.01824*.
44. Soleymani, M., Pantic, M., & Pun, T. (2011). Multimodal emotion recognition in response to videos. *IEEE transactions on affective computing*, *3*(2), 211-223.
45. Zhao, Z. Q., Zheng, P., Xu, S. T., & Wu, X. (2019). Object detection with deep learning: A review. *IEEE transactions on neural networks and learning systems*, *30*(11), 3212-3232.
46. Venkateswarlu, R. (2003, October). Eye gaze estimation from a single image of one eye. In *Proceedings Ninth IEEE International Conference on Computer Vision* (pp. 136-143). IEEE.
47. Geng, X., Zhou, Z. H., & Smith-Miles, K. (2007). Automatic age estimation based on facial aging patterns. *IEEE Transactions on pattern analysis and machine intelligence*, *29*(12), 2234-2240. Asuncion, A. and Newman, D., 2007. UCI machine learning repository.
48. Asuncion, A., & Newman, D. (2007). UCI machine learning repository.
49. Sugano, Y., Matsushita, Y., & Sato, Y. (2014). Learning-by-synthesis for appearance-based 3d gaze estimation. In *Proceedings of the IEEE conference on computer vision and pattern recognition* (pp. 1821-1828).
50. Wang, J., Tam, W. C., Jia, Y., Peacock, R., Reneke, P., Fu, E. Y., & Cleary, T. (2021). P-Flash–A machine learning-based model for flashover prediction using recovered temperature data. *Fire Safety Journal*, *122*, 103341.

51. Fu, E. Y., Tam, W. C., Wang, J., Peacock, R., Reneke, P. A., Ngai, G., Leong, H. V, & Cleary, T. (2021, May). Predicting Flashover Occurrence using Surrogate Temperature Data. In *Proceedings of the AAAI Conference on Artificial Intelligence* (Vol. 35, No. 17, pp. 14785-14794).
52. Tam, W.C., Fu, E.Y., Li, J., Peacock, R., Reneke, P., Ngai, G., Leong, H.V., Cleary, T. and Huang, M.X. (2023). Real-time flashover prediction model for multi-compartment building structures using attention based recurrent neural networks. *Expert Systems with Applications*, *223*, 119899.
53. Tam, W. C., Fu, E. Y., Peacock, R., Reneke, P., Wang, J., Li, J., & Cleary, T. (2020). Generating synthetic sensor data to facilitate machine learning paradigm for prediction of building fire hazard. *Fire technology*, 1-22.
54. Reneke, P. A., Peacock, R. D., Gilbert, S. W., & Cleary, T. (2021). CFAST–Consolidated Fire and Smoke Transport (Version 7) Volume 5: CFAST Fire Data Generator (CData). *NIST TN 1889v5. National Institute of Standards and Technology, Gaitersburg, MD*.
55. Peacock, R. D., Reneke, P. A., & Forney, G. P. (2017). CFAST–Consolidated Model of Fire Growth and Smoke Transport (Version 7) Volume 2: User's Guide. *NIST Technical Note 1889v2*.
56. McKinnon, M., Weinschenk, C., & Madrzykowski, D. (2020). Modeling Gas Burner Fires in Ranch and Colonial Style Structures. *Report. Underwriters Laboratories Inc. Columbia, MD*.
57. Tam, W. C., Fu, E. Y., Li, J., Huang, X., Chen, J., & Huang, M. X. (2022). A spatial temporal graph neural network model for predicting flashover in arbitrary building floorplans. *Engineering Applications of Artificial Intelligence*, *115*, 105258.
58. Babrauskas, V. (2016). Heat release rates. In SFPE handbook of fire protection engineering (pp. 799-904). Springer, New York, NY.
59. Vapnik, V. (1998). The support vector method of function estimation. In Nonlinear Modeling (pp. 55-85). Springer, Boston, MA.
60. Madrzykowski, D., & Weinschenk, C. (2019). Impact of fixed ventilation on fire damage patterns in full-scale structures. *National Criminal Justice Reference Service*, *252831*.
61. Reneke, P. A., Bruns, M., Gilbert, S. W., MacLaren, C. P., Peacock, R. D., Cleary, T. G., & Butry, D. T. (2019). Towards a Process to Quantify the Hazard of Fire Protection Design Alternatives.
62. Babrauskas, V. (2011). Glass breakage in fires. *Fire science and technology inc*.
63. Hurley, M. J., Gottuk, D. T., Hall Jr, J. R., Harada, K., Kuligowski, E. D., Puchovsky, M., & WIECZOREK, C. J. (Eds.). (2015). *SFPE handbook of fire protection engineering*. Springer.
64. Graves, A., & Schmidhuber, J. (2005). Framewise phoneme classification with bidirectional LSTM and other neural network architectures. *Neural networks*, *18*(5-6), 602-610.
65. Persily, A., Musser, A., & Leber, D. D. (2006). *A collection of homes to represent the US housing stock*. US NISTIR 7330. National Institute of Standards and Technology, Gaithersburg, MD.
66. Yuen, R. K., Lee, E. W., Lo, S. M., & Yeoh, G. H. (2006). Prediction of temperature and velocity profiles in a single compartment fire by an improved neural network analysis. *Fire safety journal*, *41*(6), 478-485.
67. Zhang, T., Wang, Z., Wong, H. Y., Tam, W. C., Huang, X., & Xiao, F. (2022). Real-time forecast of compartment fire and flashover based on deep learning. *Fire Safety Journal*, *130*, 103579.
68. Hodges, J. L., Lattimer, B. Y., & Luxbacher, K. D. (2019). Compartment fire predictions using transpose convolutional neural networks. *Fire Safety Journal*, *108*, 102854.

69. Fan, L., Tam, W. C., Tong, Q., Fu, E. Y., & Liang, T. (2023). An explainable machine learning based flashover prediction model using dimension-wise class activation map. *Fire Safety Journal*, 103849.
70. Wang, Z., Zhang, T., Wu, X., & Huang, X. (2022). Predicting transient building fire based on external smoke images and deep learning. *Journal of Building Engineering*, *47*, 103823.
71. Wang, Z., Ding, Y., Zhang, T., & Huang, X. (2023). Automatic real-time fire distance, size and power measurement driven by stereo camera and deep learning. *Fire Safety Journal*, 103891.
72. Wang, Z., Zhang, T., & Huang, X. (2023). Predicting real-time fire heat release rate by flame images and deep learning. *Proceedings of the Combustion Institute*, *39*(3), 4115-4123.